Directly Modulated Single-Mode Tunable Quantum Dot Lasers at 1.3 μm

Yating Wan,* Sen Zhang, Justin C. Norman, MJ Kennedy, William He, Yeyu Tong, Chen Shang, Jian-Jun He, Hon Ki Tsang, Arthur C. Gossard, and John E. Bowers

Wavelength tunable lasers are increasingly needed as key components for wavelength resource management technologies in future dense wavelength division multiplexing (DWDM) systems. While material systems with multiple quantum wells as an active region are widely used in long-wavelength tunable lasers, the unique advantages of InAs/GaAs quantum dots (QDs) for low-power operation, excellent thermal stability, and wide spectral bandwidth may open a new avenue in this field. Combining the advantages of QDs with a special designed half-wave coupled cavity structure, directly modulated, single-mode, tunable InAs/GaAs QD lasers are demonstrated at 1.3 μm wavelength range. The half-wave coupler provides an active–active coupled-cavity tunable structure without involving gratings or multiple epitaxial growths, producing synchronous power transfer in the two output waveguides and high single-mode selectivity. 27-channel wavelength switching is achieved with side-mode-suppression-ratio of around 35 dB. Under continuous-wave electrical injection, over 9 mW output power can be measured with 716 kHz Lorentzian linewidth, 4 GHz 3-dB bandwidth, and 8 Gbit s^{-1} non-return-to-zero signal modulation by directly probing the chip.

Dr. Y. Wan, Prof. A. C. Gossard, Prof. J. E. Bowers
Institute for Energy Efficiency
University of California Santa Barbara
Santa Barbara, CA 93106, USA
E-mail: yatingwan@ucsb.edu

S. Zhang, Prof. J.-J. He
State Key Laboratory of Modern Optical Instrumentation
College of Optical Science and Engineering
Zhejiang University
Hangzhou 310027, P. R. China

Dr. J. C. Norman, C. Shang, Prof. A. C. Gossard, Prof. J. E. Bowers
Materials Department
University of California Santa Barbara
Santa Barbara, CA 93106, USA

M. Kennedy, W. He, Y. Tong, Prof. J. E. Bowers
Department of Electrical and Computer Engineering
University of California Santa Barbara
Santa Barbara, CA 93106, USA

Y. Tong, Prof. H. K. Tsang
Department of Electronic Engineering
The Chinese University of Hong Kong
Shatin, Hong Kong, P. R. China

1. Introduction

With the increasing demand for high-performance, energy-efficient computing systems and data centers, optical interconnects are widely accepted as offering higher bandwidth and lower power consumption than electrical interconnects.[1] Currently, optical transmission is dominant in long-haul communications and data center networks. A similar trend is also happening at increasingly short length scales down to individual boards.[2] Vertical-cavity surface emitting lasers (VCSEL) possess high wall-plug efficiencies, GHz frequency modulation speed, and are widely adopted.[3] Further scaling to higher capacity and on-chip interconnects favors dense wavelength division multiplexing (DWDM) technology that utilizes in-plane transmitters.[4] In future DWDM systems, a widely tunable laser is one of the key components that provides dynamic wavelength management in high-traffic networks and has the additional advantage of allowing a common component stocking for inventory cost-saving and increased flexibility in building optical networks.[5]

Currently, the most common tunable lasers come in the form of either ring-based lasers,[6,7] distributed Bragg reflector (DBR) lasers,[8,9] including those integrated on Si through wafer bonding, sampled-grating distributed Bragg reflectors (SGDBR),[10] or digital super-mode DBRs[11] that are fabricated through multiple regrowth steps on native substrates. In addition to fabrication complexity, nonuniform gratings, and multiple epitaxial growths that degrade the fabrication yield, these types of lasers possess relatively large footprint and complex control algorithms for wavelength tuning with multiple electrodes. Coupled-cavity lasers have been extensively investigated since the 1980s in the form of serially coupled cavities with an etched groove.[12] However, due to the significant loss from the coupling gap and nonoptimal filter shape, the side-mode-suppression-ratio (SMSR) was limited to about 20 dB. In 2008, He et al. proposed to replace the intermediate etched groove in a coupled-cavity structure with a half-wave coupler, where an optimal cross-coupling coefficient can be achieved with an ideal π phase difference respect to the self-coupling coefficient.[13] Full C-band tuning with up to 93 channels at 50 GHz spacing and SMSR above 36 dB was demonstrated without a phase shift region and required only a single
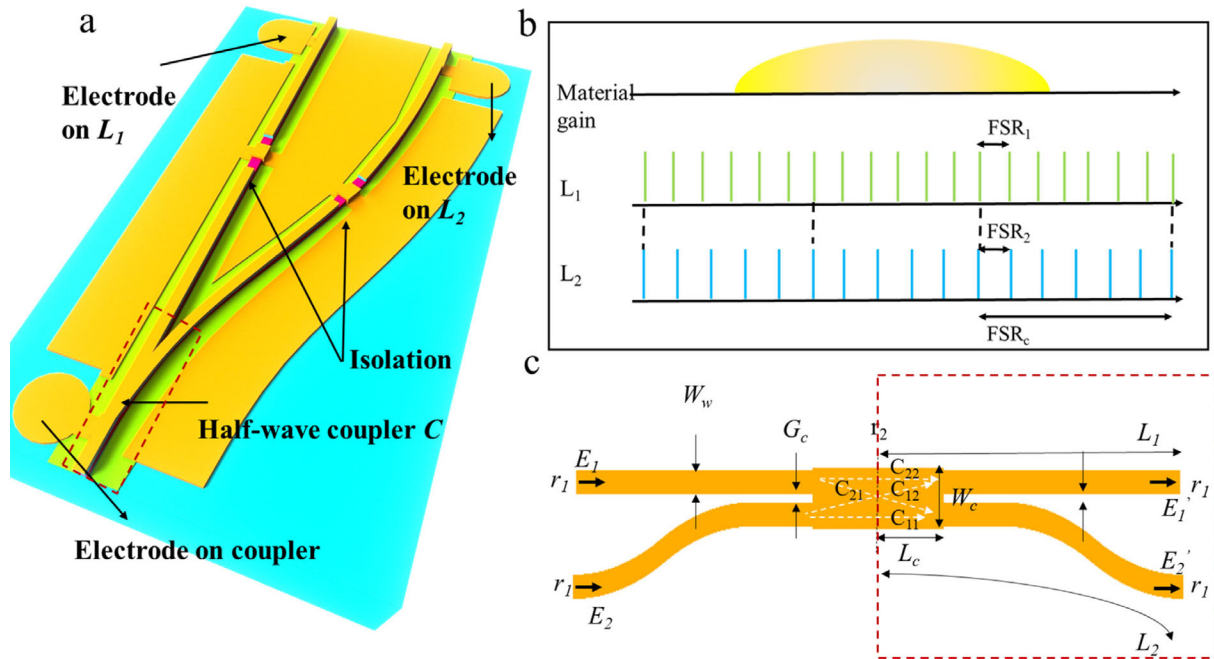
Figure 1. V-coupled cavity laser design: a) Schematic of the V-coupled cavity laser. b) Schematic diagram showing the resonant frequency combs of the two cavities and the material gain spectrum. c) Unfolded reflective 2 × 2 half-wave coupler in the V-coupled cavity laser.

electrode control for digital wavelength switching.[14] Compared to serially coupled-cavity lasers, the half-wave V-coupled cavity laser offers telecom suitable SMSR by virtue of the specially designed reflective 2 × 2 coupler, which allows the optimized cross-coupling coefficient to be much smaller than the self-coupling coefficients of both cavities while maintaining a half-wave relative phase.

Currently, two material systems with multiple quantum wells (MQW) as an active region are used for the fabrication of long-wavelength tunable lasers: $In_{(1-x-y)}Al_{(x)}Ga_{(y)}As/InP$ laser diodes and $In_{(1-x)}Ga_{(x)}As_{(y)}P_{(1-y)}/InP$ laser diodes. In both material systems, a deeply etched waveguide structure is avoided since the exposure of the active region at the sidewall will exacerbate nonradiative surface-recombination, resulting in higher thresholds and enhanced device degradation. Therefore, a shallow etched waveguide structure is typically used with weak lateral confinement such that a low-loss bend radius would exceed 1500 μm, forcing the use of etched facets.[15] In this paper, quantum dots (QDs) are adopted as the active region. By virtue of their 3D carrier confinement and characteristic density of states,[16] QDs have advantages for low threshold[17] and high-temperature operation[18] relative to their QW counterparts, allowing for deeply etched processes through reduced surface recombination.[19–22] More importantly, the insensitivity of QDs to defects and feedback offers the prospect of eliminating optical isolators in the future photonic integrated circuit (PIC) links[23] and the possibility of future laser growth and processing at 300 mm scale on Si substrates.[24–27] Combining the advantages of QDs with the half-wave coupled cavity structure, we achieved, to the best of our knowledge, the first demonstration of directly modulated single-mode tunable InAs/GaAs QD lasers in the 1.3 μm wavelength range with 27-channel wavelength switching, up to 35 dB SMSR,

over 9 mW output power, 716 kHz Lorentzian linewidth, 4 GHz 3-dB bandwidth, and 8 Gbit s^{-1} non-return-to-zero signal modulation by directly probing the chip.

2. Device Design

The tunable laser includes an all-active two-section Fabry–Pérot (FP) design (L_1, L_2) with a V-shaped half-wave coupler (C) to provide an active–active coupled-cavity tunable structure, as shown in **Figure** 1a. All of the three sections (L_1, L_2, and C) under different electrodes share the same QD structure without epitaxial regrowth or bandgap engineering, and are electrically isolated from each other by removing the heavily doped p-contact GaAs layer. The two Fabry–Pérot cavities (L_1 and L_2) possess slightly different optical path lengths of 2.5% to shape the Vernier spectrum needed for wavelength tuning, as shown in Figure 1b. With $L_1 = 1050$ μm and $L_2 = 1023$ μm, Vernier free spectral range (FSR) is determined to be 9 nm from Equations (1) and (2), where FSR_m is FSR of the mth cavity, c is the light velocity in vacuum, n_g is the effective group refractive index of the waveguide, and L is the length of the FP cavity.

$$FSR_{Vernier} = \frac{FSR_1 \times FSR_2}{|FSR_1 - FSR_2|} \tag{1}$$

$$FSR_m = \frac{c}{2n_g L} \tag{2}$$

The V-shaped coupler (C) partially coupled the light from one cavity to the other without going through a common waveguide section, that is, L_1 to L_2, or vice versa. Compared to the Y-branch

ADVANCED
SCIENCE NEWS

www.advancedsciencenews.com
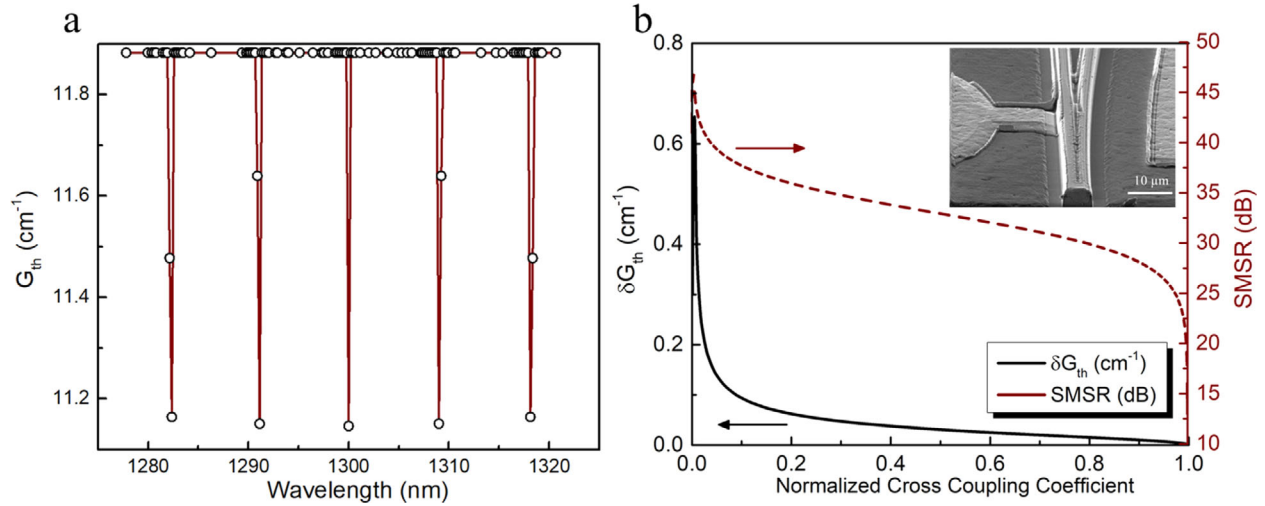
LASER
&PHOTONICS
REVIEWS

www.lpr-journal.org

Figure 2. Threshold gain calculation of the V-coupled cavity laser: a) Threshold gain difference between the lowest threshold mode and the next lowest threshold mode (left-hand) and the corresponding SMSR (right-hand) as a function of the normalized cross-coupling coefficient χ. Inset: SEM image of the half-wave coupler. b) Threshold gain spectrum of the V-coupled cavity laser when $C_{21} = 0.07$.

laser,[28] it allows the optimization of the cross-coupling coefficient with respect to the self-coupling coefficient, thus producing a higher SMSR.[13] An unfolded laser cavity with respect to the reflection plane at the closed end is shown in Figure 1c. The corresponding amplitude reflectivity (r_1, r_2) and coupling coefficients (C_{12}, C_{11}, C_{21}, C_{22}) have been labeled. By properly designing the coupler width (W_c), gap (G_c), and length (L_c), a low optimal cross-coupling coefficient can be maintained with a 180° phase difference between the two outputs of the coupler for high single-mode selectivity, as discussed below.

The wavelengths of the lasing modes as well as their threshold gain coefficients can be determined by separating the following threshold condition equation (Equation (3)) of the V-coupled cavity laser into two equations corresponding to the real and imaginary parts.[13]

$$C_{11}r_1r_2e^{2(g_1+ik_1)L_1} + C_{22}r_1r_2e^{2(g_2+ik_2)L_2}$$
$$-(C_{11}C_{22} - C_{21}C_{12})r_1^2r_1^2e^{2(g_1+ik_1)L_1}e^{2(g_2+ik_2)L_2} = 1 \qquad (3)$$

Here, k_1, k_2 ($= 2\pi n/\lambda$) and g_1, g_2 refer to the propagation constant and gain coefficient of cavity L_1, cavity L_2, respectively. The maximal threshold gain difference of 0.73 cm^{-1} between the main mode and the adjacent side modes can be achieved when $C_{12} = C_{21} = 0.07$, and $C_{11} = C_{22} = 0.93$. The corresponding threshold gain spectrum for all longitudinal modes is shown in **Figure** 2a. Using Equation (4), the SMSR can be calculated where P is the output power, γ_{tot} is the total cavity loss per centimeter, γ_m is the mirror loss of the main mode, $\Delta\gamma$ is the loss difference between the main mode, and the highest side mode, n_{sp} is the spontaneous emission factor.[29]

$$SMSR = 10\log_{10}\left[\frac{2P}{h\nu\nu_g n_{sp}\gamma_{tot}}\frac{\Delta\gamma}{\gamma_m}\right] \qquad (4)$$

In Figure 2b, the calculated SMSR is plotted together with the threshold difference as a function of the normalized coupling coefficient, which is defined in Equation (5).

$$\chi = \frac{|C_{21}|^2}{|C_{11}|^2 + |C_{21}|^2} = \frac{|C_{12}|^2}{|C_{12}|^2 + |C_{22}|^2} \qquad (5)$$

The SMSR generally increases with decreasing lasing threshold (higher-Q cavities), decreasing cavity lengths, and increasing cavity length difference. With cleaved facets, a maximum SMSR of 45 dB can be theoretically achieved for cavity lengths of $L_1 = 1050$ µm and $L_2 = 1023$ µm when the coupler (C) is designed with a length of 60 µm, a width of 6.9 µm, and a gap of 0.7 µm. This coupler design allows an optimal amount of light to be coupled from one cavity to the other, relative to the amount of light coupled back to the same cavity for high single-mode selectivity. By further considering the lithography accuracy which has a resolution of 400–450 nm and 0.25 µm alignment error, the half-wave coupler was designed with a coupler length of 40–60 µm and a gap of 0.7–1.2 µm.

3. Experimental Section

The full laser structure is schematically shown in **Figure** 3a. 1400 nm n- and p-type $Al_{0.4}Ga_{0.6}As$ cladding layers, lattice-matched to GaAs, were used for transverse optical confinement. The active region was composed of 5 layers of an InAs/In$_{0.15}$Ga$_{0.85}$As dots-in-a-well (DWELL) structures separated by 37.5 nm p-type modulation doped GaAs spacer layers designed to provide ≈10 holes per dot. The growth details have been reported.[30] Using a representative calibration sample, a dot density of 5×10^{10} cm^{-2} was measured using atomic force microscopy (AFM) and a strong luminescence at 1285 nm with a full-width at half-maximum of 28 meV was obtained from photoluminescence measurements at room temperature, as shown in
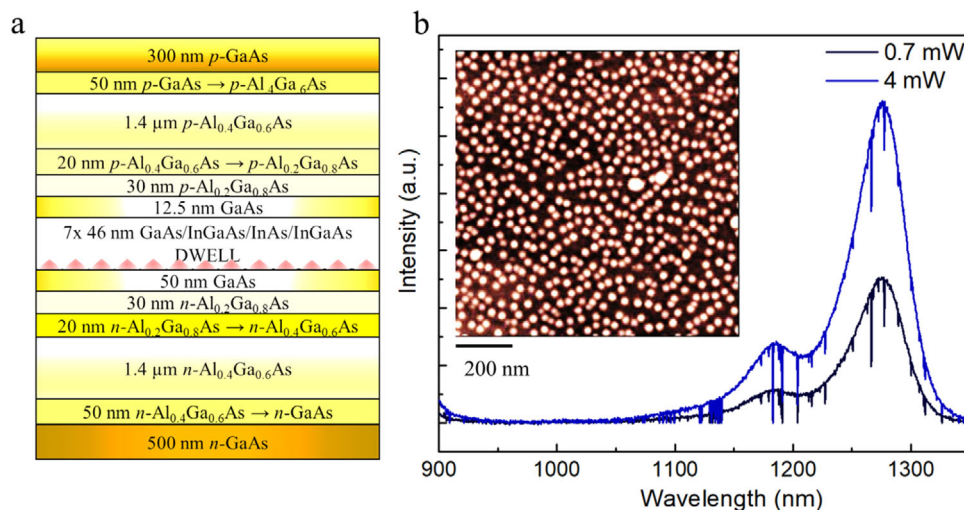
Figure 3. Epi-layer information of the QD materials: a) Schematic of the epi-layer structure. b) Photoluminescence spectrum of the as-grown sample. Inset: Atomic force microscopy image of QDs with a density of 5×10^{10} cm^{-2}. The scale bar is 200 nm.

Figure 3b. The as-grown material was then processed into deeply etched waveguide structures with an etching depth of 3.8 µm. An i-line (365 nm) step-and-repeat GCA wafer stepper was used to define the coupler shape with high resolution and critical alignment. Inductively coupled plasma with a Cl_2/N_2-based chemistry was used to etch the waveguide to achieve vertical and smooth sidewalls for low waveguide loss. After etching, the sidewall was passivated with 12 nm of Al_2O_3 by atomic-layer deposition (ALD) for the initial surface passivation, and subsequently covered with a 500-nm-thick SiO_2 layer to fully isolate the optical modes from the Pd/Ti/Pd/Au and Pd/Ge/Pd/Au metal contact stacks. The whole fabrication process proceeded in a way similar to that of a standard FP laser with the addition of an isolation etching step for separate control of the two cavities and half-wave couplers. Afterward, the laser facets were formed by cleaving with no facet coating applied to the surface. The fabricated devices were then placed and probed on a copper heat sink held at 20 °C, and a scanning electron microscopy (SEM) image is recorded in the inset in **Figure** 4a.

4. Measurement and Analysis

Figure 4a shows the light–current–voltage (L–I–V) characteristics of a representative device with a main cavity length of 1050 µm and a cavity difference of 2.5%. The injection currents on L_1, L_2 and the half-wave coupler are denoted as I_{L1}, I_{L2}, and I_c, respectively. The L–I–V curve was measured by applying a current scan of the gain section, that is, the half-wave coupler (I_c), while the injection currents on L_1 (I_{L1}), L2 (I_{L2}) were kept constant, as indicated by the legend in Figure 4a. The measured 0.9 V turn-on voltage and 6 Ω differential series resistance from the I–V curve indicate good metal contacts for efficient current injection. A threshold current of 46 mA is obtained from the L–I curve, corresponding to a threshold current density (J_{th}) of 1460 A cm^{-2}, or 208 A cm^{-2} per QD layer. The maximum output power was measured to be 9 mW at an injection current of 125 mA by an integrating sphere placed at the coupler side, and the highest wall-

plug efficiency (WPE) of 8.3% was achieved at an injection current of 102 mA. The slope efficiency (SE) was measured to be 0.14 W/A/un-coated facet and detailed gain and loss characterization of an identical active region design is presented in ref. 31. When the injection current of the half-wave coupler (I_c) was increased beyond 125 mA, the device shows power roll-off because of thermal effects. No mode hop is observed when the current on the half-wave coupler electrode is varied. When $I_{L1} = 50$ mA, $I_{L2} = 50$ mA, and $I_c = 60$ mA, a representative single mode emission centered at 1.3 µm with SMSR over 35 dB is achieved, as shown in Figure 4b. In Figure 4c, L–I curves of the same device was measured at elevated temperatures. The laser was able to function up to 35 °C under CW operation. The inset in Figure 4c presents the natural logarithm of the threshold current versus stage temperature. The dependence of threshold current on temperature follows the exponential function of $l_{th} \propto \exp(T/T_0)$, and a characteristic temperature (T_0) of 41 K is extracted. Since the measurements were under CW mode, the extracted T_0 underestimates of the true value due to junction heating but do make the results representative of performance in real-world applications.

By adjusting the injection currents on the two FP cavities synchronously while keeping injection currents I_c on the couplers fixed at 60 mA, 27 channels of tuning range with around 0.2 nm channel spacing is achieved, as shown in **Figure** 5a. The wavelength ranges from 1280.4 to 1284.75 nm with SMSR ranging from 30 to 35 dB. The designed coupler used in this device has a dimension ($W_c = 6.9$ µm, $G_c = 0.7$ µm, and $L_c = 60$ µm) that corresponds to a π phase difference and a theoretical SMSR of 45 dB. However, the coupling phase strongly depends on the coupler gap (G_c) and is also slightly affected by the coupling length L_c.[13] Considering the lithography resolution of 400–450 nm and 0.25 µm alignment error, variations in G_c during the process can deviate the coupling phase away from half-wave (i.e., 180°). Consequently, the maximal threshold gain difference decreases, resulting in a lower measured SMSR compared to the theoretical values. In the design, the Vernier tuning range (FSR$_{Vernier}$) is determined to be 9 nm from the optical path length difference of 2.5% in the coupled FP cavities. Since the material gain

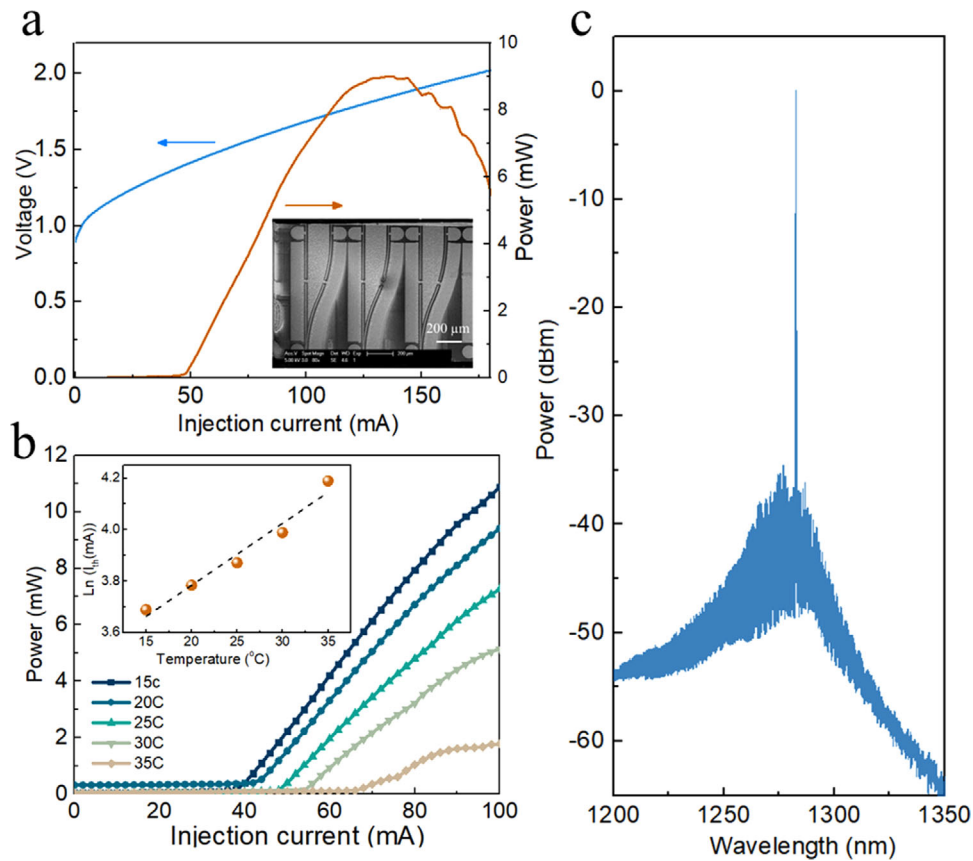**Figure 4.** a) Measured *L–I–V* curve by varying current on the half-wave coupler while keeping other sections constant; inset: SEM image of the fabricated device. b) Representative single-mode emission spectra showing an SMSR of over 35 dB. c) Temperature-dependent *L–I* curves of the same device; inset: threshold current as a function of temperature.
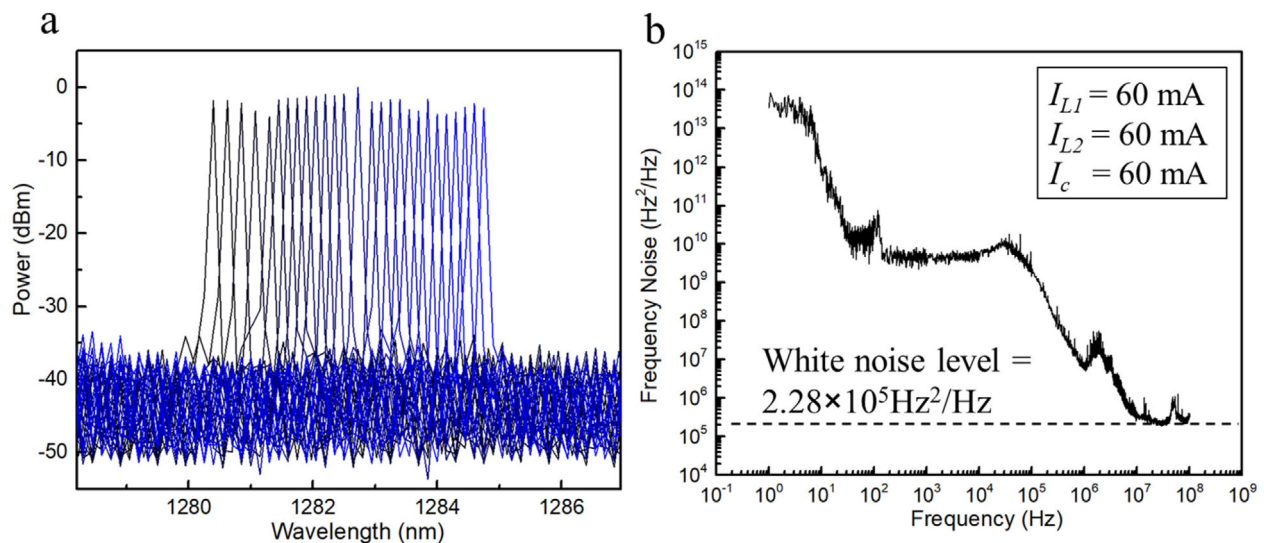

Figure 5. a) 27 channels tuning with ≈0.2 nm channel spacing. b) Frequency noise spectrum of the V-coupled cavity laser.
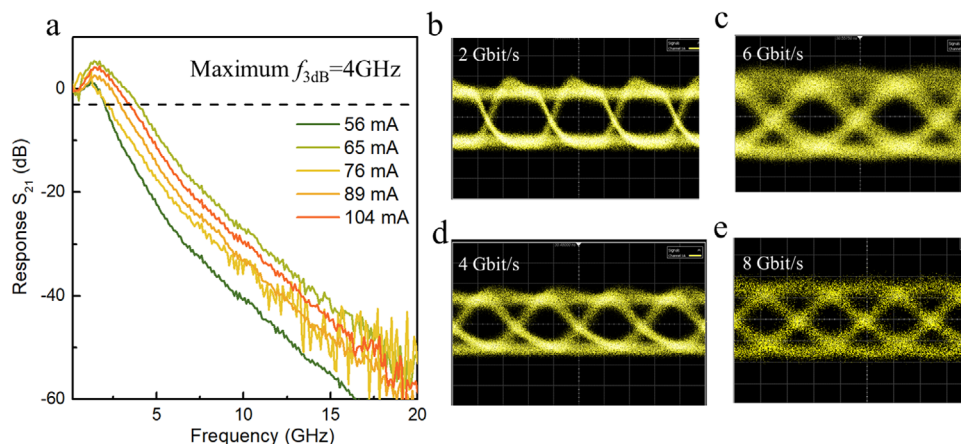
Figure 6. a) Small-signal modulation responses of the V-coupled cavity laser with coupler current biased from 56 to 104 mA. b) Eye diagrams measured at 2, 4, 6, and 8 Gbit s^{-1} by the photoreceiver with a −5 dBm received optical power. The bias current of coupler was 70 mA.

bandwidth of 52 nm is wider than the FSR$_{\text{Vernier}}$. The tuning range is limited by FSR$_{\text{Vernier}}$ determined by the optical path lengths of the two FP cavities rather than the material gain bandwidth. Currently, the tuning range is smaller than the theoretical calculated FSR$_{\text{Vernier}}$ as the refractive index variation is limited by the injection currents. In the future, with improved material gain and reduced cavity loss, the tuning range can be extended by decreasing the lengths and the length difference of the two FP cavities.

Lorentzian linewidth of the device was characterized by measuring the frequency noise spectrum using a commercial phase noise measurement system (OEWaves). When tuning the wavelength, the frequency noise spectrum shows little change and a representative spectrum recorded under the bias condition of I_{L1} = 60 mA, I_{L2} = 60 mA, and I_c = 60 mA, was shown in Figure 5b. The intrinsic linewidth, or Lorentzian linewidth of the laser can then be extracted by analyzing the frequency noise at higher frequencies where the measurement is relatively free from technical noise from electronics, vibrations, and other environmental factors, as indicated by the black dashed line. A white noise floor of $S_F(f) = 2.28 \times 10^5$ Hz^2/Hz level was measured, corresponding to a Lorentzian linewidth of $\pi \times S_F(f) = 716$ kHz.[32] It is worth mentioning that the linewidth of semiconductor lasers is closely related to the α-factor where a reduction in the absolute value of the α-factor can induce reductions in the laser linewidth by a factor of $(1+\alpha^2)$.[33] With an α-factor in the range of 2–6, traditional QW distributed feedback (DFB) or distributed Bragg reflection (DBR) lasers typically have linewidths on the order of a few megahertz.[34] For QD lasers, the α-factor is as low as 0.13, which is more than an order of magnitude lower than that of QWs.[23] It has been experimentally demonstrated that linewidths of less than 80 kHz can be achieved from 1550 nm InAs/InP QD DFB lasers with a very low reflectivity antireflection coating (AR) on both facets.[35] For ultra-narrow linewidth operation of semiconductor lasers, light coupling with high-Q resonators in external cavities is typically used, in which ultralow loss passive waveguides for mode selection and for cavity length extension are pivotal.[7,36,37] In the tunable laser reported here, the coupled cavities comprise an all-active two-section FP design, which has much higher waveguide loss compared to the typical exter-

nal cavity lasers with low loss silicon nitride or Si. Consequently, a larger linewidth is expected here compared to external cavity lasers with low-loss passive waveguides. It has been theoretically demonstrated that the smaller α-factor in QDs compared to that of QWs can be translated into a narrower linewidth with the existing narrow linewidth laser designs, including external cavities and heterogeneous Si/InP photonic platforms.[38] Therefore, significant linewidth reduction can be realized by incorporating ultralow loss passive waveguides as external cavities in the future.

The frequency response was subsequently analyzed by small signal modulation of the half-wave coupler region using a 20 GHz lightwave component analyzer (LCA, HP8703A), as shown in **Figure** 6a. The injected currents of the half-wave coupler were varied from 56 to 104 mA while the injection currents applied on the two FP cavities were fixed at 50 mA. No mode hopping was observed when we modulate the current applied to the half-wave coupler. The light output of the V-coupled cavity laser was collected by a spherical-lensed single-mode fiber and the modulated light output was detected by an internal detector of the LCA. A 3-dB bandwidth of 4 GHz was attained at a bias current of 104 mA. It is worth mentioning that InAs/GaAs QD lasers typically have direct modulation bandwidths around 10 GHz due to strong gain compression and low saturated gain.[39–43] Currently, the frequency response bandwidth of the device was limited by the relatively long cavity length and the large pad capacitance of the electrodes, which are not optimized for high-frequency operation. To further improve the bandwidth, the pad capacitance can be reduced by depositing the metals on a several micron-thick benzocyclobutene (BCB, ε = 2.6) layer. The device length can be reduced, and improved packaging could be used.

A non-return-to-zero (NRZ) pseudo-random bit sequence (PRBS) signal was used to drive the laser for back to-back (B2B) transmission. The bias current of the half-wave coupler region was fixed at 70 mA. The NRZ PRBS signal was directly generated by a programmable pattern generator (SDG Model 12070) with a peak-to-peak voltage of 1 V. QD lasers have been proved to be more stable against optical feedback as opposed to their bulk or QW counterparts owing to the small linewidth enhancement factor, the low QD size inhomogeneity, the large damping rate, and the large excited-to ground-state lasing

threshold ratio.[23] Therefore, no isolator was used during the OOK measurement. In Figure 6b, eye diagrams captured by a photoreceiver with trans-impedance amplifier (FINISAR XPRV2022A) and a sampling oscilloscope (Keysight DCA-X 86100) are presented for channel fifteen at 2, 4, 6, and 8 Gbit s^{-1}, respectively. The corresponding extinction ratios are measured to be 4.88, 4.71, 4.43, and 3.94 dB, respectively. A clear eye opening was observed up to 8 Gbit s^{-1}. Gradual closure of the eye pattern appeared due to the limited 3-dB bandwidth of the laser.

5. Conclusions

In summary, we present the design and demonstration of the first single-mode tunable InAs/GaAs QD lasers in the 1.3 µm wavelength range. Compared to existing tunable lasers utilizing multiple regrowth and subwavelength grating structures, the active–active coupled-cavity offers prominent advantages of fabrication simplicity and compactness, consuming a device size of only 1050 µm × 450 µm and can be easily fit into a small form-factor package. Compared to serial-coupled-cavity lasers, incorporation of the properly designed half-wave coupler helps to achieve telecom grade SMSR up to 35 dB with 27-channel wavelength switching. Both the tuning range and SMSR can be further improved by decreasing the cavity length and adjusting the cavity offset.[13] The emission output power is over 9 mW and can be increased by coating the two facets with high reflectivity mirrors. A 4 GHz 3-dB bandwidth and 8 Gbit s^{-1} non-return-to-zero signal modulation have been demonstrated. This can be improved by decreasing the device length and redesigning the pad distribution. The use of QD material as active region allows for a deep etching process that provides better light confinement and fabrication flexibility. In addition, the advantages of QDs in low threshold, high temperature operation, and the insensitivity to defects and optical feedback offer the prospect of utilizing this low-cost tunable laser structure in isolator-free PIC links on a Si substrate with high volume manufacturing.

Conflict of Interest

The authors declare no conflict of interest.

Keywords

coupled-cavity lasers, direct modulation, quantum dot lasers, single-mode tunable lasers

[1] M. Haurylau, G. Chen, H. Chen, J. Zhang, N. A. Nelson, D. H. Albonesi, E. G. Friedman, P. M. Fauchet, *IEEE J. Sel. Top. Quantum Electron.* **2006**, *12*, 1699.

[2] M. Smit, J. van der Tol, M. Hill, *Laser Photonics Rev.* **2012**, *6*, 1.

[3] M. Amann, W. Hofmann, *IEEE J. Sel. Top. Quantum Electron.* **2009**, *15*, 861.

[4] Q. Cheng, M. Bahadori, M. Glick, S. Rumley, K. Bergman, *Optica* **2018**, *5*, 1354.

[5] C. W. Coldren, G. A. Fish, J. S. Barton, L. Johansson, L. A. Coldren, Y. Akulova, *J. Lightwave Technol.* **2004**, *22*, 193.

[6] G. Roelkens, L. Liu, D. Liang, R. Jones, A. Fang, B. Koch, J. Bowers, *Laser Photonics Rev.* **2010**, *4*, 751.

[7] M. A. Tran, D. Huang, J. Guo, T. Komljenovic, P. A. Morton, J. E. Bowers, *IEEE J. Sel. Top. Quantum Electron.* **2019**, *26*, 1.

[8] S. Keyvaninia, G. Roelkens, D. Van Thourhout, C. Jany, M. Lamponi, A. Le Liepvre, F. Lelarge, D. Make, G.-H. Duan, D. Bordel, J.-M. Fedeli, *Opt. Express* **2013**, *21*, 3784.

[9] T. Ferrotti, B. Blampey, C. Jany, H. Duprez, A. Chantre, F. Boeuf, C. Seassal, B. B. Bakir, *Opt. Express* **2016**, *24*, 30379.

[10] V. Jayaraman, D. A. Cohen, L. A. Coldren, *Appl. Phys. Lett.* **1992**, *60*, 2321.

[11] A. J. Ward, D. J. Robbins, G. Busico, E. Barton, L. Ponnampalam, J. P. Duck, N. D. Whitbread, P. J. Williams, D. C. J. Reid, A. C. Carter, M. J. Wale, *IEEE J. Sel. Top. Quantum Electron.* **2005**, *11*, 149.

[12] W. T. Tsang, *Semicond. Semimetals* **1985**, *22*, 257.

[13] J.-J. He, D. Liu, *Opt. Express* **2008**, *16*, 3896.

[14] J. Meng, X. Xiong, H. Xing, H. Jin, D. Zhong, L. Zou, J. Zhao, J.-J. He, *IEEE Photonics Technol. Lett.* **2017**, *29*, 1035.

[15] S. Cheung, J. Matres, M. R. Tan, *J. Lightwave Technol.* **2019**, *37*, 2133.

[16] J. C. Norman, D. Jung, Y. Wan, J. E. Bowers, *APL Photonics* **2018**, *3*, 030901.

[17] S. Chen, W. Li, J. Wu, Q. Jiang, M. Tang, S. Shutts, S. Elliott, A. Sobiesierski, A. Seeds, I. Ross, P. Smowton, H. Liu, *Nat. Photonics* **2016**, *10*, 307.

[18] J. Kwoen, B. Jang, K. Watanabe, Y. Arakawa, *Opt. Express* **2019**, *27*, 2681.

[19] Y. Wan, J. Norman, Q. Li, M. Kennedy, D. Liang, C. Zhang, D. Huang, Z. Zhang, A. Liu, A. Torres, D. Jung, A. Gossard, E. Hu, K. Lau, J. Bowers, *Optica* **2017**, *4*, 940.

[20] N. V. Kryzhanovskaya, A. E. Zhukov, M. V. Maximov, E. I. Moiseev, I. I. Shostak, A. M. Nadtochiy, Y. V. Kudashova, A. A. Lipovskii, M. M. Kulagina, S. I. Troshkov, *IEEE J. Sel. Top. Quantum Electron.* **2015**, *21*, 709.

[21] T. Zhou, M. Tang, G. Xiang, X. Fang, X. Liu, B. Xiang, S. Hark, M. Martin, M. Touraton, T. Baron, Y. Lu, S. Chen, H. Liu, Z. Zhang, *Optica* **2019**, *6*, 430.

[22] Y. Wan, Q. Li, A. Y. Liu, W. W. Chow, A. C. Gossard, J. E. Bowers, E. Hu, K. M. Lau, *Appl. Phys. Lett.* **2016**, *108*, 221101.

[23] J. Duan, H. Huang, B. Dong, D. Jung, J. C. Norman, J. E. Bowers, F. Grillot, *IEEE Photonics Technol. Lett.* **2019**, *31*, 345.

[24] Q. Feng, W. Wei, B. Zhang, H. Wang, J. Wang, H. Cong, T. Wang, J. J. Zhang, *Appl. Sci.* **2019**, *9*, 385.

[25] Y. Wan, Q. Li, A. Y. Liu, A. C. Gossard, J. E. Bowers, E. Hu, K. M. Lau, *Opt. Lett.* **2016**, *41*, 1664.

[26] Z. Zhou, B. Yin, J. Michel, *Light: Sci. Appl.* **2015**, *4*, e358.

[27] Y. Wang, S. Chen, Y. Yu, L. Zhou, L. Liu, C. Yang, M. Liao, M. Tang, Z. Liu, J. Wu, W. Li, I. Ross, A. J. Seeds, H. Liu, S. Yu, *Optica* **2018**, *5*, 528.

[28] J.-O. Wesström, G. Sarlet, S. Hammerfeldt, L. Lundqvist, P. Szabo, P.-J. Rigole, in *Optical Fiber Communication Conf. on CD-ROM*, Optical Society of America, Washington, DC **2004**, p. TuE2.

[29] T. L. Koch, U. Koren, *J. Lightwave Technol.* **1990**, *8*, 274.

[30] Y. Wan, D. Inoue, D. Jung, J. C. Norman, C. Shang, A. C. Gossard, J. E. Bowers, *Photonics Res.* **2018**, *6*, 776.

[31] J. C. Norman, Z. Zhang, D. Jung, C. Shang, M. Kennedy, M. Dumont, R. W. Herrick, A. C. Gossard, J. E. Bowers, *IEEE J. Quantum Electron.* **2019**, *1*, 1.

[32] K. Kikuchi, T. Okoshi, *IEEE J. Quantum Electron.* **1985**, *21*, 669.

[33] D. Jung, Z. Zhang, Y. Wan, S. Liu, C. Shang, R. W. Herrick, W. W. Chow, A. C. Gossard, J. E. Bowers, *IEEE J. Quantum Electron.* **2019**, *55*, 1.

[34] U. T. Schwarz, E. Sturm, W. Wegscheider, V. Kümmler, A. Lell, V. Härle, *Appl. Phys. Lett.* **2003**, *83*, 4095.

[35] J. Duan, H. Huang, Z. G. Lu, P. J. Poole, C. Wang, F. Grillot, *Appl. Phys. Lett.* **2018**, *112*, 121102.

[36] C. Xiang, W. Jin, J. Guo, J. D. Peters, M. Kennedy, J. Selvidge, P. A. Morton, J. E. Bowers, *Optica* **2020**, *7*, 20.

[37] H. Guan, A. Novack, T. Galfsky, Y. Ma, S. Fathololoumi, A. Horth, T. N. Huynh, J. Roman, R. Shi, M. Caverley, Y. Liu, T. Baehr-Jones, K. Bergman, M. Hochberg, *Opt. Express* **2018**, *26*, 7920.

[38] Z. Zhang, D. Jung, J. Norman, W. W. Chow, J. E. Bowers, *IEEE J. Sel. Top. Quantum Electron.* **2019**, *25*.

[39] D. Inoue, D. Jung, J. Norman, Y. Wan, N. Nishiyama, S. Arai, A. C. Gossard, J. E. Bowers, *Opt. Express* **2018**, *26*, 7022.

[40] Y.-H. Jhang, R. Mochida, K. Tanabe, K. Takemasa, M. Sugawara, S. Iwamoto, Y. Arakawa, *Opt. Express* **2016**, *24*, 18428.

[41] A. E. Zhukov, M. V Maksimov, A. R. Kovsh, *Semiconductors* **2012**, *46*, 1225.

[42] C. Shang, Y. Wan, J. C. Norman, N. Collins, I. MacFarlane, M. Dumont, S. Liu, Q. Li, K. M. Lau, A. C. Gossard, J. E. Bowers, *IEEE J. Sel. Top. Quantum Electron.* **2019**, *25*, 1.

[43] Y. Wan, J. Norman, J. Bowers, in *Future Directions in Silicon Photonics* (Eds: S. Lourdudoss, J. E. Bowers, C. Jagadish), Semiconductors and Semimetals Vol *101*, Academic Press, San Diego, CA **2019**, p. 305.